The excitation of CO in CO-dominated cometary comae

M. Żółtowski, F Lique, J. Loreau, A Faure, M. Cordiner

The excitation of CO in CO-dominated cometary comae

M. Żółtowski,[1,2] F. Lique,[2]★ J. Loreau,[3] A. Faure,[4] M. Cordiner[5,6]
[1]LOMC - UMR 6294, CNRS-Université du Havre, 25 rue Philippe Lebon, BP 1123, F-76063 Le Havre, France.
[2]Univ Rennes, CNRS, IPR (Institut de Physique de Rennes) - UMR 6251, F-35000 Rennes, France.
[3]KU Leuven, Department of Chemistry, B-3001 Leuven, Belgium.
[4]Univ. Grenoble Alpes, CNRS, IPAG, 38000 Grenoble, France.
[5]Astrochemistry Laboratory, NASA Goddard Space Flight Center, 8800 Greenbelt Road, Greenbelt, MD 20771, USA.
[6]Department of Physics, Catholic University of America, Washington, DC 20064, USA.

Accepted XXX. Received YYY; in original form ZZZ

ABSTRACT

An abundance of CO significantly surpassing the abundance of H_2O is observed in the comae of comets at large heliocentric distances. In these environments, CO molecules can be the most abundant species and they may be therefore the dominant projectiles inducing collisional excitation of the cometary molecules. It is thus of high interest to investigate the excitation of CO by CO. This article provides a new set of CO–CO collisional rate coefficients for temperatures up to 150 K and for CO rotational levels j_1 up to 10. These data are obtained from quantum scattering calculations using the coupled states approximation. They are used in a simple radiative transfer model in order to test their impact on the excitation of cometary CO. Because mutual (de-)excitations of the target and projectile are important, the CO projectile was assumed to be thermalized at the kinetic temperature. We found that the non-LTE regime extends for CO densities in the range $10^3 - 10^7$ cm^{-3}. We also observed that as soon as the CO/H2O ratio is larger than 70%/30%, the contribution of H_2O collisions can be neglected. Similarly, the excitation of CO by CO may be ignored for relatively low CO/H_2O density ratios (≤30%/70%). Finally, when the coma is a ∼50%/50% mixture of CO and H_2O, the contribution of both colliders is similar and has to be considered.

Key words: molecular data – scattering – comets: general

1 INTRODUCTION

Comets spend most of their lives far away from the Sun. Therefore they carry molecular ices that were present during the formation of our Solar system. When they approach the Sun, cometary nuclei release these molecules into an expanding atmosphere (coma). Observing these molecules gives us insight into the chemical and physical conditions at the epoch of comet and giant planet formation. It is then essential to analyze observations of cometary comae as precisely as possible (Cochran et al. 2015).

The most abundant constituent of cometary comae is usually H_2O. Thus, H_2O is often used as a reference to which we compare abundances of the other cometary molecules. The next most abundant molecules observed in typical comets at heliocentric distances of ∼1 au (Bockelée-Morvan et al. 2004; Bockelée-Morvan & Biver 2017) are respectively CO_2 (up to 30% relative to H_2O), CO (up to 25% relative to H_2O), and CH_3OH (up to 7% relative to H_2O). The abundances of the other molecules usually do not exceed 1% (Bockelée-Morvan & Biver 2017).

However, there are some peculiar comets observed at large heliocentric distances where the production rates of CO and CO_2 are higher than H_2O. For example, in the 29P/Schwassmann-Wachmann 1 comet observed at a heliocentric distance within ∼ 2.5 au, the production of CO molecules was found to be 5 times larger than that of H_2O (Ootsubo et al. 2012). In the C/2016 R2 (PanSTARRS) comet recently observed at a heliocentric distance of ∼ 2.8–2.9 au, the CO/H_2O abundance ratio was estimated to be ∼ 170, a ratio 37 times larger than the highest CO/H_2O ratio ever observed (Cordiner et al. 2022). This dominance in the production of CO compared to H_2O is explained by the differences in the CO and H_2O sublimation temperatures (Womack et al. 2017). Indeed, the H_2O ices start to sublimate once the comet approaches our inner solar system within the distance of ∼ 3 au (H_2O molecules having a relatively high sublimation temperature of ∼ 150 K) while CO (with a much lower sublimation temperature of ∼ 20 – 30 K) starts to sublimate at much larger distance from the Sun, where H_2O is still frozen in the comet nucleus. Therefore, a high CO/H_2O production rate ratio exceeding unity is observed when the comets are observed at large distance (≥ 3 a.u) from the sun, where the radiation field and nucleus temperature are expected to be weak. Hence, in such comets, the main constituant and then collisional partner for the excitation of cometary molecules is not H_2O but other volatile molecules such as CO or CO_2 (Womack et al. 2017; Marboeuf & Schmitt 2014, and references therein).

The physical conditions in a cometary atmosphere prevent local thermodynamical equilibrium (LTE) to be sustained in the whole coma. Non-LTE excitation/radiative transfer models for comets have been developed for decades and we refer the reader to the Chapter

★ E-mail: francois.lique@univ-rennes1.fr

by Bodewits et al. (2022) for a recent review. In the following, we will address processes that govern the excitation and emission of CO molecules in the (sub)millimetre range, i.e. CO rotational levels within the ground vibrational state, using a simple excitation model. Going beyond the LTE approximation requires to take into account both radiative and collisional processes. Radiative data for cometary molecules are usually well known from laboratory spectroscopy. At the opposite, collisional data require long and expensive (in terms of memory and CPU time) calculations (Roueff & Lique 2013). In the case of comets, the most important collisional systems involve mutual interactions between CO, CO_2, and H_2O molecules.

Some of these systems have been already the object of molecular scattering studies. Unfortunately they are computationally too complex to be studied with the almost exact quantum close coupling scattering theory (Arthurs & Dalgarno 1960) and some approximations had to be applied. For the H_2O–H_2O collisional system, Buffa et al. (2000) used a semi-classical treatment based on the dipole-dipole interaction to derive cross sections. For the same system, Semenov & Babikov (2017) extended the semi-classical approach to include quadrupole interactions and their methodology was tested against the more sophisticated mixed quantum/classical MQCT calculations of (Boursier et al. 2020). In the case of CO–H_2O, a first set of data was obtained in the 1990s from line shape measurement by Green (1993). Recently Faure et al. (2020) provided a more accurate data set of rate coefficients for the CO–H_2O collisions using the statistical adiabatic channel method (SACM) (Loreau et al. 2018). For the CO–CO collisional system, data between the first five rotational levels were provided by Ndengué et al. (2015) combining both time-independent and approximate time-dependent quantum scattering approaches.

In a previous work by some of us (Cordiner et al. 2022), a preliminary set of CO−CO collisional rate coefficients computed with a full quantum time-independent method but limited to $T = 5-30$ K and $j = 0 - 6$) was published. This data set was extended recently (Żółtowski et al. 2022, hereafter Paper I) to temperatures $T = 5 - 100$ K and to the transitions between rotational levels $j = 0 - 7$. In the present paper, we provide a new extension of these data sets in order to cover temperatures up to 150 K and transitions between levels up to $j = 10$ for more general use in models. In addition, the new collisional data are used in a simple radiative transfer model of cometary comae (Faure et al. 2020; Loreau et al. 2022) in order to test their impact on the excitation of CO. We note that since CO–CO is a system of identical molecules, the distinction between 'target' and 'projectile' is artificial. To our knowledge, however, public radiative transfer codes do not allow to treat the internal structure of a target and a projectile on equal footing. The common and convenient artefact of target and projectile will be therefore used below, but we will test the sensitivity of the CO (target) population to the actual CO projectile internal states. Finally, we will investigate the impact of different CO/H_2O abundance ratios on the CO (target) level population.

Our article is organized as follows. In section 2, we present the results of our new scattering calculations. In section 3, we discuss the impact of our new collisional data on the non-LTE excitation of CO in cometary comae. In section 4, conclusions are drawn.

2 CO–CO COLLISIONAL RATE COEFFICIENTS

As written in the introduction, we aim here at extending the CO–CO collisional rate coefficients of Paper I to both higher temperatures and higher rotational energy levels. The CO–CO interaction potential and the scattering methodology is essentially the same as in paper I and we refer the reader to this paper for details. Briefly, the four dimensional CO–CO rigid rotor potential energy surface calculated by Vissers et al. (2003) was used in our calculations and state-to-state cross sections were calculated with the Molscat scattering code (Hutson & Green 1994). We consider the two colliding species as distinguishable species. We used the coupled states (CS) approximation (McGuire & Kouri 1974) that was shown to be accurate for collision energies above 50 cm^{-1}. In the following, j_1 refers to the rotational level of the CO considered as the target and j_2 refers to the rotational level of the CO considered as the projectile. The rotational basis used in the calculations contains all energy levels with $j_1 = j_2 \leq 15$. Such a rotational basis is large enough to converge to better than 10% inelastic cross sections between levels up to $j_1 = j_2 = 10$. The cross section calculations were performed for total energies up to 1200 cm^{-1}. This energy range allows to calculate state-to-state rate coefficients for temperatures up to 150 K :

$$k_{j_1 j_2 \rightarrow j_1' j_2'}(T) = \left(\frac{8}{\pi \mu k_B^3 T^3}\right)^{\frac{1}{2}} \int_0^\infty \sigma_{j_1 j_2 \rightarrow j_1' j_2'}(E_c) E_c e^{-\frac{E_c}{k_B T}} dE_c \quad (1)$$

where, μ is reduced mass of the system, k_B is the Boltzmann constant, $\sigma_{j_1 j_2 \rightarrow j_1' j_2'}$ is the cross section for the transition $(j_1, j_2) \rightarrow (j_1', j_2')$ and E_c is collisions energy.

In Fig. 1, state-to-state de-excitation rate coefficients are provided at 50 and 150 K. First, we can observe that the values of the rate coefficients decrease with increasing Δj_1 and/or Δj_2, in agreement with the energy gap law, as already discussed in paper I. In addition, for a given Δj_1 transition, the rate coefficients increase with increasing Δj_2. Such behaviour means that the internal energy released by the target is efficiently transferred to the projectile and can be explained by the preference in conserving the collision energy, which implies a conservation of the total internal energy. Finally, we found a significant propensity rule in favor of transitions with $\Delta j_1 = -\Delta j_2$ (transitions with a strict conservation of the internal energy). Such transitions would be purely elastic if the CO molecules were considered indistinguishable in the scattering calculations. This explains the dominance of such transitions in our approach. We did not find any particular temperature dependence of the propensity rules, as expected from the weak temperature dependence of the rate coefficients (see Paper I).

In order to assess the impact of the excitation of the projectile on the magnitude of the rate coefficients, we have computed the 'effective' rate coefficients (Phillips et al. 1996) as follows:

$$k_{j_1 \rightarrow j_1'; j_2}(T) = \sum_{j_2'=0}^{10} k_{j_1 j_2 \rightarrow j_1' j_2'}(T) \quad (2)$$

Figure 2 presents effective de-excitation rate coefficients $k_{j_1 \rightarrow 0; j_2}$ at 10, 50 and 100 K. As one can see, these rate coefficients are decreasing with increasing j_2. Indeed, the rotational energy spacing increases with increasing j_2, which leads to smaller rate coefficients (energy gap law). At the exception of the effective rate coefficients for $j_2 = 0$, the variation of the effective rate coefficients with increasing j_2 is moderate and we do not observe any large differences between effective rate coefficients with $j_2 > 2$.

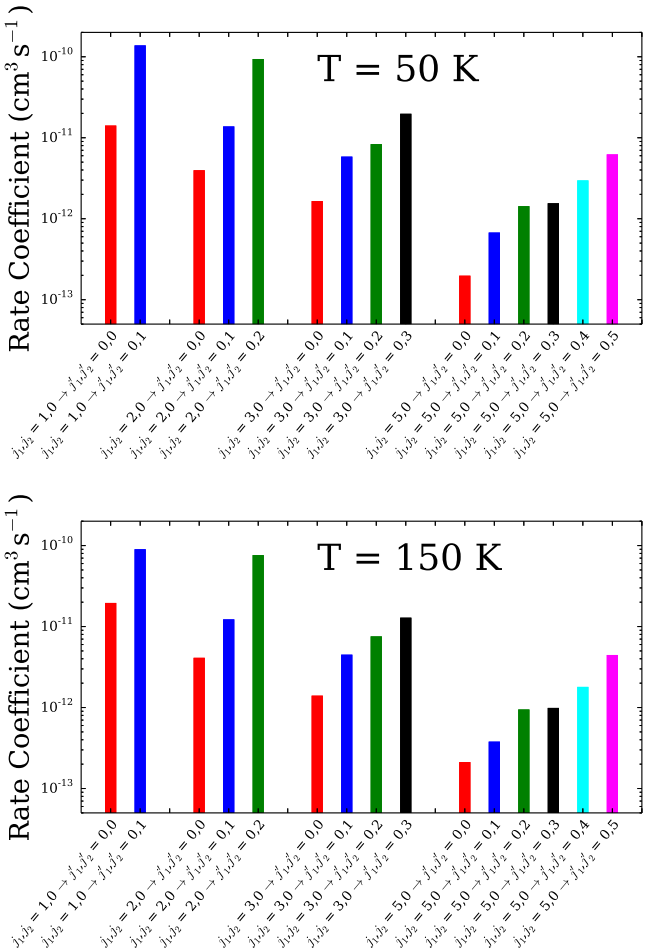

Figure 1. Selective state-to-state rate coefficients at 50 K(upper panel) and 150 K (lower panel).

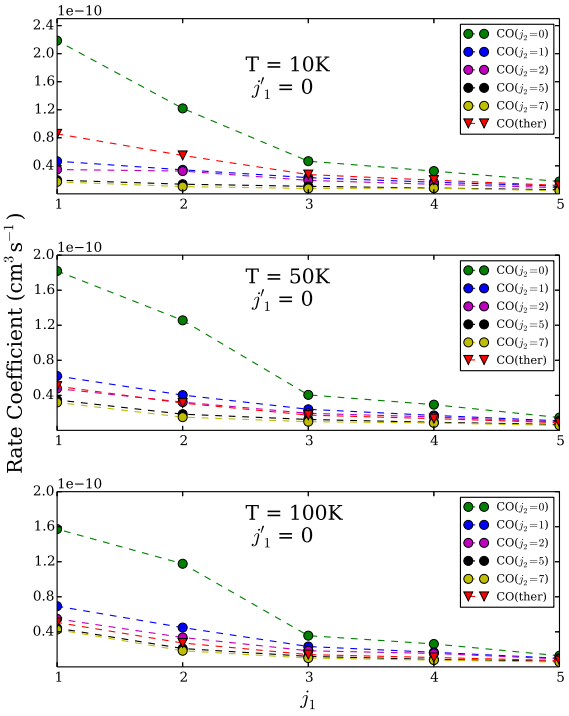

Figure 2. Comparison of effective rate coefficients where the initial projectile's rotational state was fixed at j_2 = 0, 1, 2, 5 and 7, and summed over all possible final states of projectile. De-excitation transitions to the ground state (j'_1 = 0) from the first five excited rotational states are presented. The thermalized set of rate coefficients is also plotted for comparison.

3 ASTROPHYSICAL MODELING

To assess the impact of the new collisional data on the astrophysical modeling of cometary comae, we performed radiative transfer calculations to simulate the excitation of CO in CO-dominated comae.

Non-LTE radiative transfer calculations were performed with the RADEX code (van der Tak et al. 2007) using the escape probability approximation at steady-state. In the radiative transfer calculations, we consider only radiative and collisional processes in order to model the relative population of the CO rotational levels, i.e. state-selective reactive processes such as photodissociation are neglected. All models presented in this work were performed assuming the typical physical conditions for a CO-dominated coma at an heliocentric distance R = 3 au (see below). In order to describe the density profile of CO molecules in the coma, we used a classic Haser model (Haser 1957) which is expressed by the following formula:

$$n_{CO}(r) = \frac{Q_{CO}}{4\pi r^2 v} e^{(-r\frac{\beta_{CO}}{v})} \quad (3)$$

where r is the nucleocentric distance, Q_{CO} is the production rate of the CO molecules fixed at 10^{28} s^{-1}, v is the expansion velocity fixed at 0.46 km/s, and β_{CO} is the CO photodissociation rate fixed at 2.1× 10^{-7} s^{-1} at R = 3 au. The density profile of CO molecules is presented in Fig. 3. Our non-LTE model assumes that the CO rotational population in the coma is at steady-state at a given CO density, i.e. at a given r.

The CO target column density N(CO) was not computed self-consistently but was fixed at 10^{14} cm^{-2}. This value corresponds to $r \sim 10^3 - 10^4$ km in the above Haser model, Eq. 3, i.e. to the non-LTE regime (see Fig. 3). As discussed in Faure et al. (2020), the relative populations are not sensitive to the column density provided that N(CO) < 10^{16} cm^{-2}, i.e. as long as the lines are optically thin and photon trapping (self-absorption) is not important. The line width was thus set at 0.92 km/s which corresponds to twice the expansion velocity for comets at heliocentric distance of 3 a.u (Dello Russo et al. 2016). We vary the density of the CO projectile from 10^1 to 10^9 cm^{-3}. This density range corresponds to nucleocentric distances of a few tens to a few 10^5 km (see Fig. 3). We considered 3 different kinetic temperatures: 10, 50, and 100 K. For the radiation field, we used the cosmic microwave background (CMB) combined with the solar radiation as described in Faure et al. (2020) but adjusted to the distance R = 3 au. Our model includes the lowest 80 ro-vibrational levels of CO. Their relative energies and the corresponding transition Einstein coefficients were taken from the HITRAN data base (Gordon et al. 2022). Since our scattering calculations were performed only for transitions between the first 11 lowest rotational levels of CO (j = 0 – 10), the rate coefficients for transitions implying higher energy levels were simply set to zero. The validity of such approximation is justified by the fact that the population of these levels is negligibly small for the physical conditions investigated here (Faure et al. 2020).

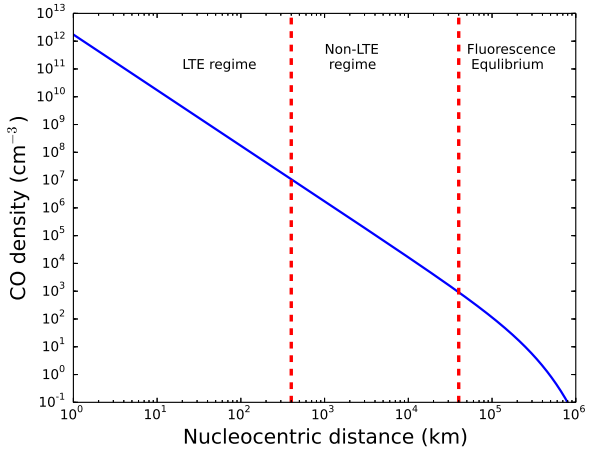

Figure 3. Density profile of the CO molecules in the comet at an heliocentric distance of 3 au, as given by the Haser model. The production rate of CO molecule was set to $Q_{CO} = 10^{28}$ s^{-1}, and the photodissociation rate to $\beta_{CO} = 2.1\times 10^{-7}$ s^{-1} (at $R = 3$ au). The dashed line separate (starting from the left side), the LTE regime, non-LTE regime, and Fluorescence regime.

3.1 Determining a suitable set of CO–CO collisional rate coefficients

Standard radiative transfer codes such as RADEX distinguish between the target and the projectile and they neglect the internal structure of the latter, i.e. the possibility of the projectile to be (de-)excited. This approach is not suited for collisions between identical molecules since mutual (de)excitation of the target and the projectile is allowed. Nevertheless, in order to perform RADEX calculations, a set of CO–CO collisional data where the population of the CO projectile is fixed was necessary.

Usually, when considering a projectile with an internal structure, e.g. H_2, the rate coefficients are taken for a given rotational state j_2 of the projectile that is conserved during the collision such that $j_2 = j_2'$. This approach is valid for inelastic collisions induced by H_2 at low temperature since, due to large energy spacings ($\geq$ 510 K), the probability of H_2 excitation remains small up to $\sim$ 500 K. This is however questionable in the case of collisions induced by heavier projectiles such as CO since they can be easily (de-)excited during the collisional process, even at 10 K, due to small energy spacings ($\geq$ 5.53 K in CO). As an alternative, the rate coefficients can be averaged over a given distribution of the projectile and summed over its final levels. Considering that detailed balance between excitation and de-excitation rate coefficients is imposed in RADEX, the rate coefficients can only be averaged over a thermal distribution of the projectile:

$$k_{j_1\to j_1'}(T) = \sum_{j_2=0}^{10} n_{j_2}(T) \sum_{j_2'=0}^{10} k_{j_1 j_2\to j_1' j_2'}(T) \tag{4}$$

$$n_{j_2}(T) = \frac{(2j_2+1)e^{\frac{-E_{j_2}}{k_B T}}}{\sum_{j_2'=0}^{10}(2j_2'+1)e^{\frac{-E_{j_2'}}{k_B T}}} \tag{5}$$

where $n_{j_2}(T)$ is the thermal population of the projectile at a temperature T and E_{j_2} is the energy of a rotational level j.

Indeed, the detailed balance relation for scattering between two molecules is the following:

$$k_{j_1 j_2\to j_1' j_2'}(T) = \frac{(2j_1'+1)(2j_2'+1)}{(2j_1+1)(2j_2+1)} e^{\frac{(E_{j_1}-E_{j_1'}+E_{j_2}-E_{j_2'})}{k_B T}} k_{j_1' j_2'\to j_1 j_2}(T) \tag{6}$$

If these full state-to-state rate coefficients are averaged over a thermal distribution of rotational states of the projectile at the kinetic temperature T and summed over the final rotational states of the projectile, one does obtain the detailed balance relation for the target:

$$k_{j_1\to j_1'}(T) = \frac{(2j_1'+1)}{(2j_1+1)} e^{\frac{(E_{j_1}-E_{j_1'})}{k_B T}} k_{j_1'\to j_1}(T). \tag{7}$$

We insist that $n_{j_2}(T)$ needs to be a thermal distribution, i.e. must obey Eq. 5. Any other rotational distribution of the projectile (even thermal but at a temperature different from the kinetic temperature) leads to a set of rate coefficients that do not fulfill the detailed balance relation.

In order to test the impact of different rotational distributions of the CO projectile on the level population of the CO target, we performed radiative transfer calculations considering either a projectile in a given and unchanged rotational state ($j_2 = 0$ or 5) or assuming a thermal rotational distribution of the projectile (Eq. 4). Results are presented in Fig. 4.

As one can see, the differences between the three distributions of j_2 are very significant. These differences simply originate from the magnitude of the set of rate coefficients used in the radiative transfer calculations, the thermally averaged data being much larger than the others. Indeed, as discussed in the previous section, the rate coefficients with excitation or de-excitation of both the target and the projectile exhibit a higher magnitude than those with the excitation of only one CO molecule. Hence, fixing the rotational state of the projectile leads to a significant underestimation of the CO target excitation in a CO-dominated gas. As a consequence, while fixing the projectile in one given rotational state is an attractive approach in terms of implementation (as it obeys detailed balance), it is not recommended in the case of heavy projectile (with energy spacings smaller than the kinetic temperature T) due to the importance of mutual excitations between the target and the projectile.

In order to include the possibility of (de-)excitation of the projectile, one can use the effective rate coefficients and play with the rotational distribution of the projectile, e.g. by defining a rotational temperature (T_{rot}) for the projectile different from the kinetic temperature T. Collisional rate coefficients are thus computed using Eq. 4, with the n_{j_2} population being calculated for $T_{rot} \neq T$. We stress again that such set of rate coefficients does not fulfill the detailed balance relation and so the actual excitation and de-excitation rate coefficients must be employed in radiative transfer calculations. We performed some preliminary tests and found that T_{rot} has a significant impact on the CO target population, the best compromise being to use the thermally averaged rate coefficients, i.e. when $T_{rot} = T$. Thus, while the thermally averaged rate coefficients agree within a factor 2 with the effective rate coefficients (see Fig. 2), the rotational temperature of the projectile plays a non-negligible role in the population of the target. As a result, the full state-to-state rate coefficients (i.e. those defined in Eq. (6)) should be used to solve the (non-linear) statistical equilibrium equations in order to simultaneously solve for the (identical) target and projectile populations. This non-standard problem should be investigated in future works.

In what follows, on we will use the thermally averaged set of rate coefficients, as in Faure et al. (2020) for CO–H_2O.

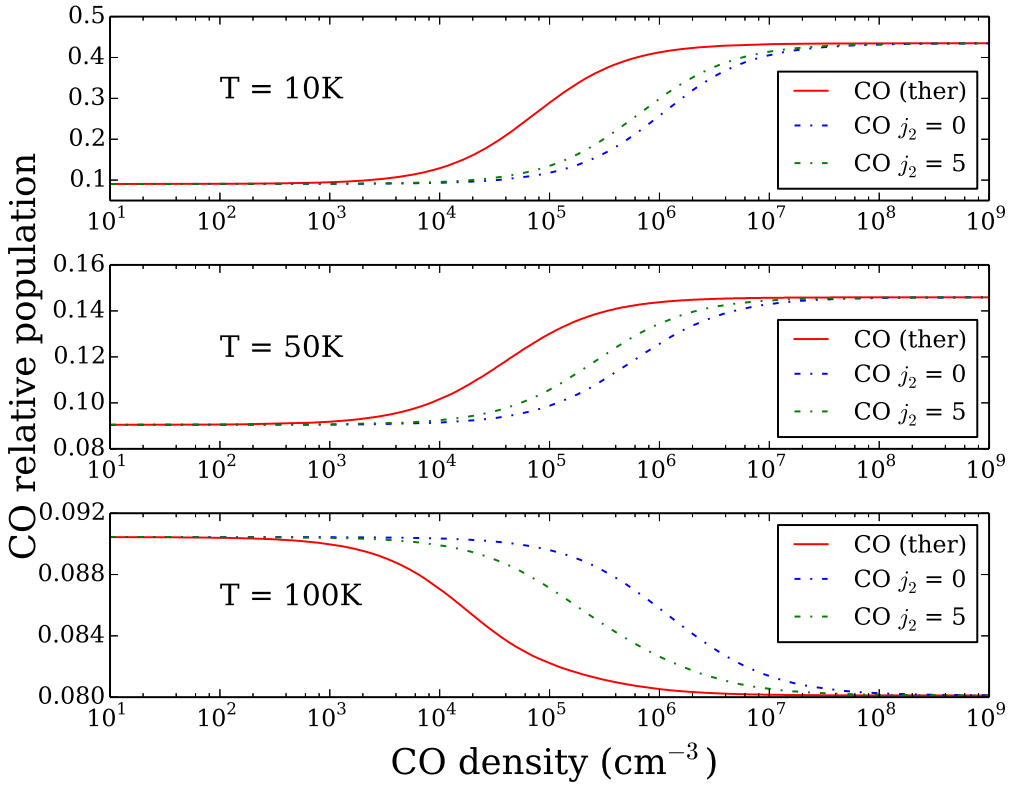

Figure 4. CO relative population of the $j_1 = 1$ state as a function of CO (projectile) density. The excitation of CO is induced by collisions with a thermally averaged projectile (red solid line), a projectile in $j_2 = j_2' = 0$ state (blue dashed line) and a projectile in $j_2 = j_2'$ == 5 state (green dashed dotted line). Calculations were preformed at kinetic temperatures of 10, 50 and 100 K.

3.2 Impact of the new data

The results of our non-LTE models are presented in Fig. 5 where the population of levels j_1 is plotted as function of the CO density for kinetic temperatures of 10, 50, and 100 K.

From Fig. 5, we can clearly distinguish three different regimes for all plotted levels (see Fig. 3). The LTE regime will apply for density of CO molecules higher than $\approx 10^7$ cm^{-3} which corresponds to distances $r \leq 400$ km from the nuclei of the comet. The 'non-LTE' regime (seee below) exists for CO densities in the $10^3 - 10^7$ cm^{-3} range which corresponds to nucleocentric distances from $\sim$ 400 km to $\sim$ 40,000 km. For density lower than 10^3 cm^{-3} and then nucleocentric distances higher than 40,000 km, the fluorescence equilibrium is established. Thus, although fluorescence equilibrium is also a non-LTE regime, what we call here the non-LTE region of the coma lies between the thermal and fluorescence equilibrium limits. We also notice from Fig. 5 that the density range corresponding to the non-LTE regime does not significantly vary with temperature at the opposite of the level populations that are strongly dependent on the temperature (in the LTE and non-LTE regime).

As we mentioned in the introduction, H_2O is usually the most abundant molecule in the coma of comets. Therefore, we now compare the excitation of CO induced by collisions with H_2O to the excitation of CO induced by CO. For the CO–H_2O rate coefficients, we used the thermalized set of collisional rate coefficients of Faure et al. (2020). It should be noted that Faure et al. (2020) did not find any significant differences for the excitation of CO induced by ortho- or by para-H_2O.

At first, we compare in Fig. 6 the two sets of rate coefficients at three kinetic temperatures of 10, 50, and 100K, for de-excitation transitions to the ground rotational level of CO. As one can see, the similarities between the two sets of rate coefficients is high. The highest differences are observed for $\Delta j_1 = 1$ transitions but the deviations remain within a factor 2. One can also notice that the CO–CO rate coefficients are slightly larger than those for CO–H_2O in the case of transitions with small Δj_1 whereas the reverse is seen for large Δj_1. The CO–H_2O interaction potential well is significantly larger than the CO–CO one and this may explain the larger coupling between rotational states with large Δj_1.

Finally, we investigated the impact of different CO/H_2O abundance ratios on the population of the CO molecules. We thus performed radiative transfer calculations to determine the CO population in a cometary coma containing both CO and H_2O. We used the following abundance ratios of projectiles: H_2O = 100%, CO/H_2O = 30% / 70%, CO/H_2O = 70% / 30%, and CO = 100%. In Fig. 7, we present results for the $j_1 = 1$ level of CO. We chose only one of the H_2O nuclear-spin symmetry for our modeling, *para*-H_2O.

For all three kinetic temperatures considered, populations obtained from the 4 abundance ratios agree relatively well, with however some significant differences. A similar pattern is observed for all j_1 levels of CO despite different temperature effects. Thus, we note that the deviation between models with 0 and 30% of H_2O (red and blue) are minor, suggesting that it is reasonable in CO-dominated comae to neglect the contribution of H_2O collisions. Similarly, for H_2O-dominated comae where the CO/H_2O ratio is lower than 30%/70%,

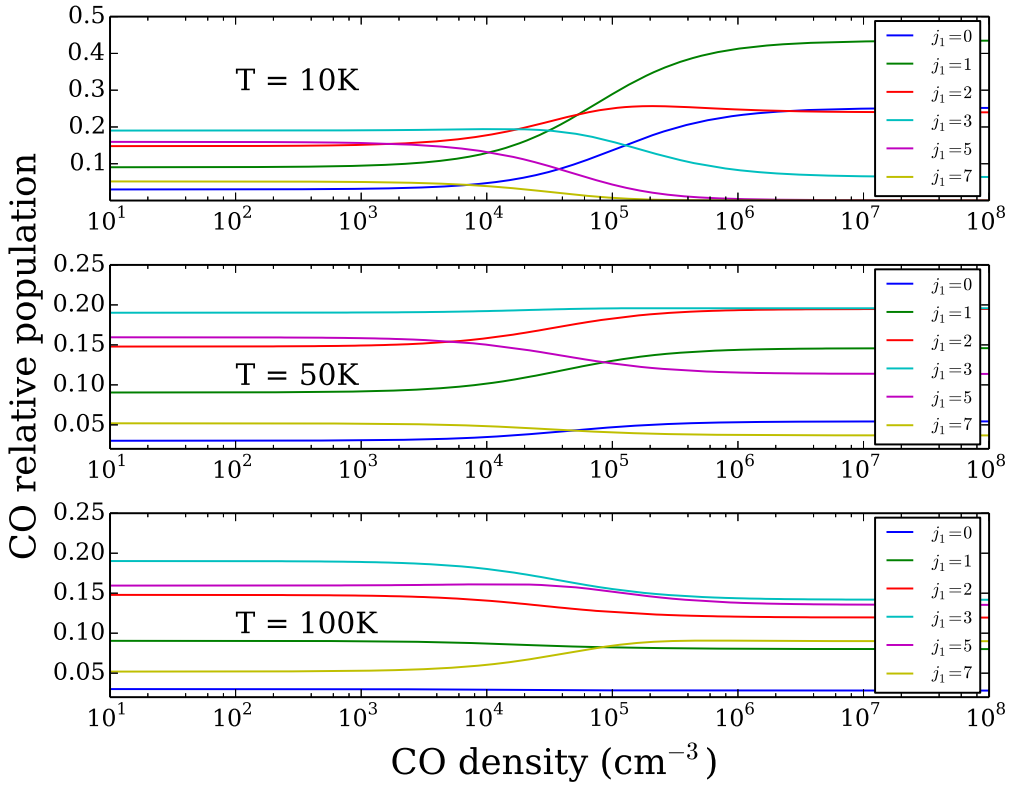

Figure 5. Level populations of CO (j_1=0, 1, 2, 3, 5, 7) as functions of CO density for temperatures of 10, 50, and 100 K.

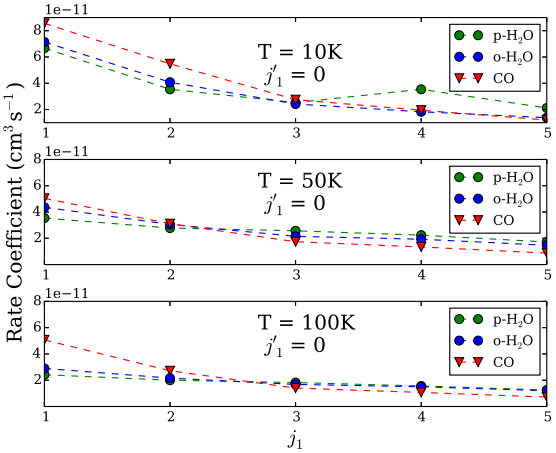

Figure 6. De-excitation transitions to the ground state ($j'_1 = 0$) from the first five excited rotational states are presented. The CO data are from this work, the H_2O data were taken from Faure et al. (2020).

the excitation induced by CO does not play a significant role and can be neglected. We note that when the coma is a ~50%/50% mixture of CO and H_2O, the contribution of both colliders is similar and has to be considered. Such a situation might be encountered for CO-rich comets observed at heliocentric $1 < R < 3$ au.

4 CONCLUSIONS

We have presented new collisional rate coefficients for the CO–CO collisional system. Data are provided for the transitions between rotational energy levels of the CO molecule up $j_1 = 10$ and for temperatures up to 150 K. The new set of rate coefficients was used in radiative transfer models of CO- and also H_2O-dominated comae. The results indicate that using a set of rate coefficients thermally averaged over the CO projectile is the best approximation so far because mutual excitations between CO target and CO projectile are important. We also found that the non-LTE regime extends for CO densities in the $10^3 - 10^7$ cm^{-3} range. Finally, we observed that as soon as the CO/H_2O ratio is larger than 70%/30%, the contribution of H_2O collisions can be neglected. For a recent review of CO/H_2O ratios in comets, the reader is referred to Biver et al. (2022).

These new collisional data should allow a better modeling of the CO column density and physical conditions in CO-dominated comae. We note, however, that we have used thermalized rate coefficients, i.e. assuming that the projectile is thermalized at the kinetic temperature. This is obviously a convenient but crude approximation. In future works, the full state-to-state rate coefficients should be used when solving the statistical equilibrium in order to treat the target and projectile on similar footing. This is required for systems with identical molecules such as CO–CO, H_2O–H_2O and CO_2–CO_2, of interest in comets. It will be thus necessary to test various numerical methods and approximations.

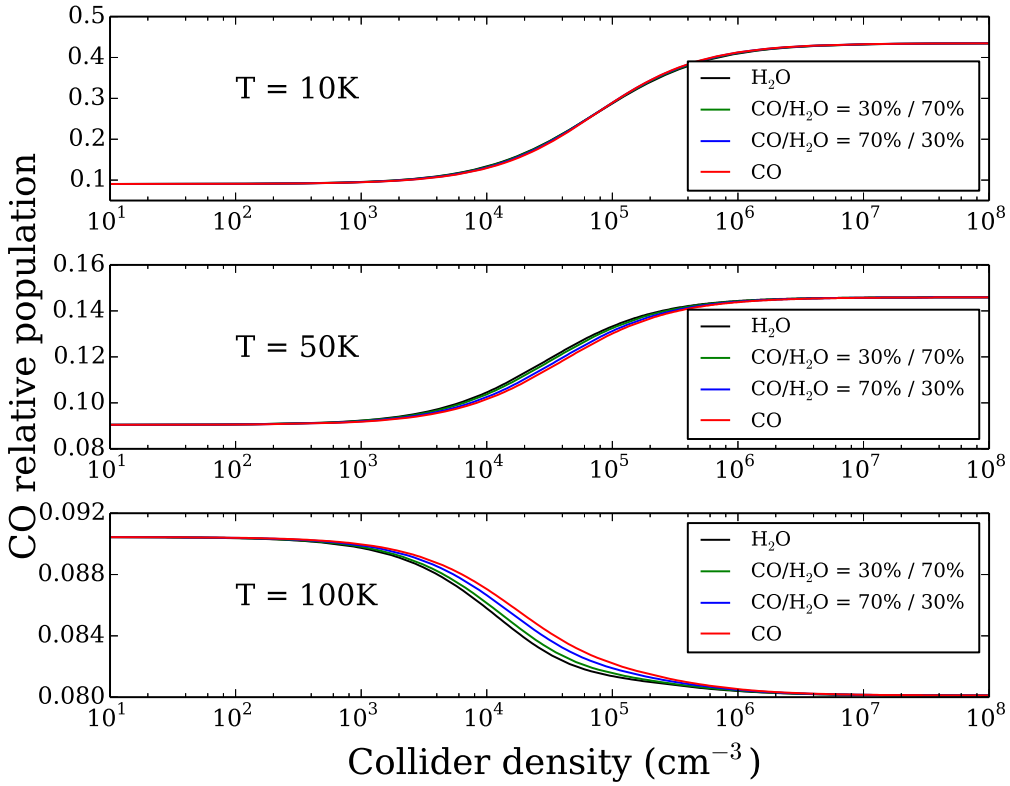

Figure 7. CO relative population for level $j_1 = 1$, as a function of the total density of the projectiles, for different CO and H_2O relative abundances. Calculations were preformed at three kinetic temperatures, 10K - upper graph, 50K - middle graph, and 100K bottom graph. The black line presents results obtain with an abundance ratio CO/H_2O= 0%/100%, green line with CO/H_2O = 30%/70 %, blue line with CO/H_2O = 70% /30 %, and red line with CO/H_2O=100%/0%.

ACKNOWLEDGEMENTS

F.L. acknowledges Rennes Metropole for financial support. This research was supported by the CNRS national program 'Physique et Chimie du Milieu Interstellaire'. J.L. acknowledges support from Internal Funds KU Leuven through Grant No. 19-00313. M.A.C was supported by the National Science Foundation under Grant No. AST-2009253. We wish to acknowledge the support from the CEA/GENCI for awarding us access to the TGCC/IRENE supercomputer within the A0110413001 project and from Wroclaw Centre for Networking and Supercomputing.

DATA AVAILABILITY

The data underlying this article will be made available through the EMAA[1], LAMDA (Schöier et al. 2005; van der Tak et al. 2020) and BASECOL (Dubernet, M.-L. et al. 2013) data bases. They are also available on request.

REFERENCES

Arthurs A. M., Dalgarno A., 1960, Proc. R. Soc. London, Ser. A, 256, 540

Biver N., Dello Russo N., Opitom C., Rubin M., 2022, arXiv, arXiv:2207.04800

Bockelée-Morvan D., Biver N., 2017, Philos Trans R Soc Lond A, 375, 20160252

Bockelée-Morvan D., Crovisier J., Mumma M. J., Weaver H. A., 2004a, in Festou M. C., Keller H. U., Weaver H. A., eds, , Comets II. p. 391

Bodewits D., Bonev B. P., Cordiner M. A., Villanueva G. L., 2022, arXiv, arXiv:2209.02616

Boursier C., Mandal B., Babikov D., Dubernet M. L., 2020, MNRAS, 498, 5489

Buffa G., Tarrini O., Scappini F., Cecchi-Pestellini C., 2000, ApJS, 128, 597

Cochran A., et al., 2015, Space Science Reviews, 197

Cordiner M. A., et al., 2022, ApJ, 929, 38

Daniel F., Dubernet M.-L., Grosjean A., 2011, A&A, 536, A76

Dello Russo N., Kawakita H., Vervack R. J., Weaver H. A., 2016, Icarus, 278, 301

Dubernet, M.-L. et al., 2013, A&A, 553, A50

Faure A., Lique F., Loreau J., 2020, MNRAS, 493, 776

Gordon I., et al., 2022, J. Quant. Spect. Rad. Trans., 277, 107949

Green S., 1993, ApJ, 412, 436

Haser L., 1957, Bulletin de la Société Royale des Sciences de Liege, 43, 740

Hutson J., Green S., 1994, CCP6, Daresbury

Loreau J., Lique F., Faure A., 2018, ApJ, 853, L5

Loreau J., Faure A., Lique F., 2022, MNRAS 516, 5964

Marboeuf U., Schmitt B., 2014, Icarus, 242, 225

McGuire P., Kouri D. J., 1974, J. Chem. Phys., 60, 2488

Ndengué S. A., Dawes R., Gatti F., 2015, J. Phys. Chem. A, 119, 7712

Ootsubo T., et al., 2012, ApJ, 752, 15

Phillips T. R., Maluendes S., Green S., 1996, Astrophys. J. Supp. Series, 107, 467

Roueff E., Lique F., 2013, Chem. Rev., 113, 8906

Schöier F. L., van der Tak F. F. S., van Dishoeck E. F., Black J. H., 2005,

[1] https://emaa.osug.fr/,

A&A, 432, 369
Semenov A., Babikov D., 2017, J. Phys. Chem. A, 121, 4855
Vissers G. W. M., Wormer P. E. S., van der Avoird A., 2003, Phys. Chem. Chem. Phys., 5, 4767
Womack M., Sarid G., Wierzchos K., 2017, PASP, 129, 031001
van der Tak F. F. S., Black J. H., Schöier F. L., Jansen D. J., van Dishoeck E. F., 2007, A&A, 468, 627
van der Tak F. F. S., Lique F., Faure A., Black J. H., van Dishoeck E. F., 2020, Atoms, 8, 15
Żółtowski M., Loreau J., Lique F., 2022, Phys. Chem. Chem. Phys., 24, 11910

This paper has been typeset from a TEX/LATEX file prepared by the author.